One-dimensional pion, kaon, and proton femtoscopy in Pb-Pb collisions at √sNN = 2.76 TeV

(ALICE Collaboration) Adam, J.; ...; Antičić, Tome; ...; Erhardt, Filip; ...; Gotovac, Sven; ...; Mudnić, Eugen; ...; ...

PHYSICAL REVIEW C **92**, 054908 (2015)

One-dimensional pion, kaon, and proton femtoscopy in Pb-Pb collisions at $\sqrt{s_{NN}} = 2.76$ TeV

J. Adam *et al.**
(ALICE Collaboration)
(Received 30 July 2015; published 19 November 2015)

The size of the particle emission region in high-energy collisions can be deduced using the femtoscopic correlations of particle pairs at low relative momentum. Such correlations arise due to quantum statistics and Coulomb and strong final state interactions. In this paper, results are presented from femtoscopic analyses of $\pi^{\pm}\pi^{\pm}$, $K^{\pm}K^{\pm}$, $K^0_S K^0_S$, pp, and $\overline{p}\overline{p}$ correlations from Pb-Pb collisions at $\sqrt{s_{NN}} = 2.76$ TeV by the ALICE experiment at the LHC. One-dimensional radii of the system are extracted from correlation functions in terms of the invariant momentum difference of the pair. The comparison of the measured radii with the predictions from a hydrokinetic model is discussed. The pion and kaon source radii display a monotonic decrease with increasing average pair transverse mass m_T which is consistent with hydrodynamic model predictions for central collisions. The kaon and proton source sizes can be reasonably described by approximate m_T scaling.

DOI: 10.1103/PhysRevC.92.054908 PACS number(s): 25.75.Dw, 24.10.Nz, 25.75.Ag

I. INTRODUCTION

Two-particle correlations at low relative momenta (commonly referred to as *femtoscopy*), which are sensitive to quantum statistics (in the case of identical particles) as well as strong and Coulomb final-state interactions (FSIs), are used to extract the space-time characteristics of the particle-emitting sources created in heavy-ion collisions [1–3]. The source radii extracted from these correlations describe the system at kinetic freeze-out, i.e., the last stage of particle interactions. Pion femtoscopy, which is the most common femtoscopic analysis, has shown signatures of hydrodynamic flow in heavy-ion collisions, manifesting as a decrease in the source radii with increasing transverse mass $m_T = \sqrt{k_T^2 + m^2}$ [4,5], where $k_T = |\mathbf{p}_{T,1} + \mathbf{p}_{T,2}|/2$ is the average transverse momentum of the pair. This behavior can be interpreted as one of the signatures of the formation of deconfined quark matter in these collisions [6]. However, a necessary condition for collective behavior is for *all* particles created in the collision, not just pions, to experience hydrodynamic flow. Thus, femtoscopic studies with particles other than pions are also needed. It was shown that the hydrodynamic picture of nuclear collisions for the particular case of small transverse flow leads to the same m_T behavior of the longitudinal radii (R_{long}) for pions and kaons [7]. This common m_T scaling for π and K is an indication that the thermal freeze-out occurs simultaneously for π and K and that these two particle species are subject to the same Lorentz boost. Previous kaon femtoscopy studies carried out in Pb-Pb collisions at the SPS by the NA44, NA49, and CERES Collaborations [8–10] reported the decrease of R_{long} with m_T as $\sim m_T^{-0.5}$ as a consequence of the boost-invariant longitudinal flow. Subsequent studies carried out in Au-Au collisions at RHIC [11–13] have shown the same level in the m_T dependencies for π and K radii, consistent with a common freeze-out hypersurface. Like the SPS analysis, no exact universal m_T scaling for the three-dimensional (3D) radii was observed at RHIC. In the case of the one-dimensional correlation radius R_{inv}, only approximate scaling with m_T is expected as an additional confirmation of hydrodynamic expansion [4]. In fact, R_{inv} source sizes as a function of m_T for different particle types (π, K, p...) follow the common curve with an accuracy of $\sim$10%.

The motivation for comparing femtoscopic analyses with different particle species is not limited to studying m_T dependence. The kaon analyses also offer a cleaner signal compared to pions, as they are less affected by resonance decays, while the proton analysis provides a possibility for checking if baryons are included in the collective motion. Studying charged and neutral kaon correlations together provides a convenient experimental consistency check, since they require different detection techniques (charged tracks vs decay vertex reconstruction) and call for different final-state interaction fitting parametrizations (Coulomb dominated vs strong interaction dominated), yet they are predicted to exhibit the same femtoscopic parameters [14]. In addition to the charged kaon analyses at the SPS and RHIC, neutral kaon correlations were studied in Au-Au collisions at RHIC [15], and ALICE has performed analyses on both charged and neutral kaons in pp collisions [16,17]. Recent pion femtoscopic results were obtained at RHIC [18] and the LHC [5,19–21], and proton femtoscopy has also been previously studied at RHIC [22].

This paper presents the results of femtoscopic studies of $\pi^{\pm}\pi^{\pm}$, $K^{\pm}K^{\pm}$, $K^0_S K^0_S$, pp, and $\overline{p}\overline{p}$ correlations from Pb-Pb collisions at $\sqrt{s_{NN}} = 2.76$ TeV by the ALICE experiment at the LHC. The femtoscopic radii and λ parameters (the latter describe the decrease of the femtoscopic correlations due to, e.g., long-lived resonances; see Secs. III A and IV) are extracted from one-dimensional correlation functions in terms of the invariant momentum difference for a range of collision centralities and m_T values. A hydrokinetic model [14] is used to compare the kaon experimental results with hydrodynamic predictions.

*Full author list given at the end of the article.

The organization of the paper is as follows. In Sec. II, we describe the data selection criteria. In Sec. III, the details of the correlation functions and the fitting process are discussed. The results of the analysis are shown in Sec. IV, and a summary is provided in Sec. V.

II. DATA ANALYSIS

The dataset analyzed in this paper is from Pb-Pb collisions at $\sqrt{s_{NN}} = 2.76$ TeV at the LHC measured by the ALICE detector [23]. About 8 million events from 2010 and about 40 million events from 2011 were used (2010 data were analyzed in the pion and K^0_S analyses only). Events were classified according to their centrality determined using the measured amplitudes in the V0 detectors [24]. Charged particle tracking is generally performed using the time projection chamber (TPC) [25] and the inner tracking system (ITS) [23]. The ITS allows for high spatial resolution in determining the primary (collision) vertex. In the pion, charged kaon, and proton analyses, the determination of the momenta of the tracks was performed using tracks reconstructed with the TPC only and constrained to the primary vertex. Primary tracks were selected based on the distance of closest approach (DCA) to the primary vertex. Additional track selections based on the quality of the track reconstruction fit and the number of detected "hit" points in the TPC were used. Also, all primary pairs sharing more than 5% of TPC clusters were rejected. In the neutral kaon analysis, the secondary daughter tracks used global (TPC and ITS) track reconstruction and did not use any cuts based on track reconstruction quality or number of used or shared TPC clusters. The secondary vertex finder used to locate the neutral kaon decays employed the "on-the-fly" reconstruction method [26], which recalculates the daughter track momenta during the original tracking process under the assumption that the tracks came from a decay vertex instead of the primary vertex.

Particle identification (PID) for reconstructed tracks was carried out using both the TPC and the time-of-flight (TOF) detector [27] in the pseudorapidity range $|\eta| < 0.8$. For TPC PID, a parametrized Bethe-Bloch formula was used to calculate the specific energy loss (dE/dx) in the detector expected for a particle with a given mass and momentum. For PID with TOF, the particle mass was used to calculate the expected time-of-flight as a function of track length and momentum. For each PID method, a value N_σ was assigned to each track denoting the number of standard deviations between the measured track information and the calculations mentioned above. Different cut values of N_σ were chosen based on detector performance for the various particle types and track momentum (see Table I for specific values used in each analysis) [28].

The analysis details specific to each particle species used in this study are discussed separately below.

A. Pion selection

The main single-particle selection criteria used in the pion analysis are summarized in Table I. Pion identification was performed using the TPC only. An overall purity of the pion candidate sample was estimated using TPC dE/dx distributions of the data and was found to be above 95%. The main source of contamination comes from $e^{\pm}$ in the region where the dE/dx curves for pions and electrons intersect.

TABLE I. Single-particle selection criteria.

Pion selection	
Transverse momentum p_T	$0.14 < p_T < 2.0$ GeV/c
$\|\eta\|$	< 0.8
Transverse DCA to primary vertex	< 0.2 cm
Longitudinal DCA to primary vertex	< 0.15 cm
$N_{\sigma,\mathrm{TPC}}$	< 3
Charged kaon selection	
p_T	$0.15 < p_T < 1.5$ GeV/c
$\|\eta\|$	< 0.8
Transverse DCA to primary vertex	< 2.4 cm
Longitudinal DCA to primary vertex	< 3.0 cm
$N_{\sigma,\mathrm{TPC}}$ (for $p < 0.5$ GeV/c)	< 2
$N_{\sigma,\mathrm{TPC}}$ (for $p > 0.5$ GeV/c)	< 3
$N_{\sigma,\mathrm{TOF}}$ (for $0.5 < p < 0.8$ GeV/c)	< 2
$N_{\sigma,\mathrm{TOF}}$ (for $0.8 < p < 1.0$ GeV/c)	< 1.5
$N_{\sigma,\mathrm{TOF}}$ (for $1.0 < p < 1.5$ GeV/c)	< 1.0
Neutral kaon selection	
$\|\eta\|$	< 0.8
Daughter-daughter $\mathrm{DCA_{3D}}$	< 0.3 cm
$\mathrm{DCA_{3D}}$ to primary vertex	< 0.3 cm
Decay length	< 30 cm
Cosine of pointing angle	> 0.99
Invariant mass	$0.480 < m_{\pi^+\pi^-} < 0.515$ GeV/c^2
Daughter p_T	> 0.15 GeV/c
Daughter $\|\eta\|$	< 0.8
Daughter $\mathrm{DCA_{3D}}$ to primary vertex	> 0.4 cm
Daughter $N_{\sigma,\mathrm{TPC}}$	< 3
Daughter $N_{\sigma,\mathrm{TOF}}$ (for $p > 0.8$ GeV/c)	< 3
Proton selection	
p_T	$0.7 < p_T < 4.0$ GeV/c
$\|\eta\|$	< 0.8
Transverse DCA to primary vertex	< 2.4 cm
Longitudinal DCA to primary vertex	< 3.2 cm
$N_{\sigma,\mathrm{TPC}}$ (for $p < 0.8$ GeV/c)	< 3
$\sqrt{N^2_{\sigma,\mathrm{TPC}} + N^2_{\sigma,\mathrm{TOF}}}$ (for $p > 0.8$ GeV/c)	< 3

Femtoscopic correlation functions of identical particles are sensitive to the two-track reconstruction efficiency because the correlated particle pairs (i.e., those with small relative momentum) generally have close trajectories. The main two-track issues are splitting (two tracks reconstructed from one particle) and merging (one track reconstructed from two particles), which are generally avoided using a track separation cut. For pions, pairs were required to have a separation of $|\Delta\eta| > 0.016$ or $\sqrt{\Delta\eta^2 + \Delta\varphi^{*2}} > 0.045$ measured at the radial distance 1.2 m. Here, η is the pseudorapidity, and φ^* is the azimuthal coordinate taking into account track bending due to the magnetic field.

B. Charged kaon selection

The main single-particle selection criteria used in the charged kaon analysis are listed in Table I. $K^{\pm}$ identification

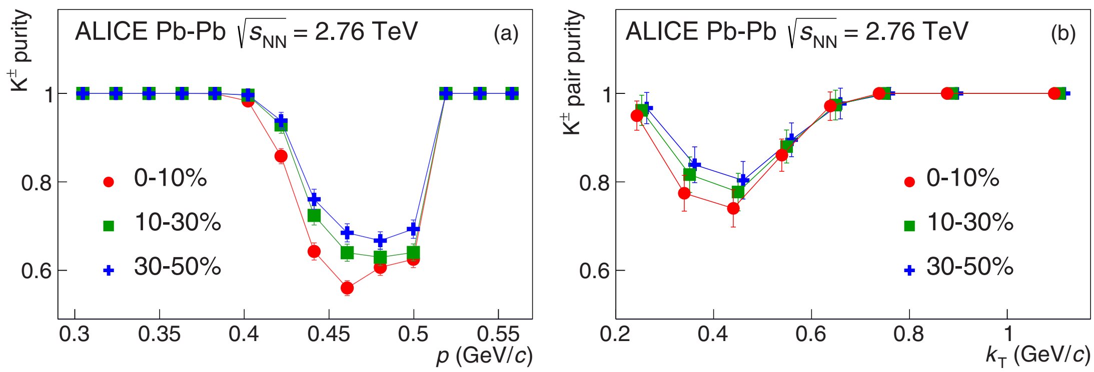

FIG. 1. (Color online) Single $K^{\pm}$ purity (a) and $K^{\pm}$ pair purity (b) for different centralities. In (b) the k_T values for different centrality intervals are slightly offset for clarity.

was performed using the TPC (for all momenta) and TOF (for $p > 0.5$ GeV/c) detectors. Figure 1(a) shows the momentum dependence of the single kaon purity, defined as the fraction of accepted kaon tracks that correspond to true kaon particles. The purity values were obtained from TPC dE/dx distributions of the data and by studying HIJING [29] simulations using GEANT3 [30] to model particle transport through the detector. Like the pions, the dominant contamination for charged kaons in the momentum region $0.4 < p < 0.5$ GeV/c comes from $e^{\pm}$. The pair purity is calculated as a product of two single-particle purities, where the momenta are taken from the experimental distribution. The $K^{\pm}$ pair purity as a function of k_T for three different centralities is shown in Fig. 1(b).

Regarding two-track selection criteria, charged kaon pairs were required to have a separation of $|\Delta\eta| > 0.02$ or $|\Delta\varphi^*| > 0.017$ measured at the radial distance 1.6 m.

C. Neutral kaon selection

The decay channel $K^0_S \rightarrow \pi^+\pi^-$ was used for the identification of neutral kaons. The single-particle cuts for parents (K^0_S) and daughters ($\pi^{\pm}$) used in the decay-vertex reconstruction are shown in Table I. PID for the pion daughters was performed using both TPC (for all momenta) and TOF (for $p > 0.8$ GeV/c). Figure 2 shows an example of the $\pi^+\pi^-$ invariant mass distribution where the K^0_S peak is seen. The cuts used in this analysis were chosen to balance statistics and signal purity. The neutral kaon purity (defined as Sig./[Sig.+Bkg.] for $0.480 < m_{\pi^+\pi^-} < 0.515$ GeV/c^2) was found to be greater than 0.95.

Two main two-particle cuts were used in the neutral kaon analysis. To resolve two-track inefficiencies associated with the daughter tracks, such as the splitting or merging of tracks discussed above, a separation cut was employed in the following way. For each kaon pair, the spatial separation between the same-sign pion daughters was tabulated at several points throughout the TPC (every 20 cm radially from 85 to 245 cm) and averaged. If the average separation of either pair of tracks was below 5 cm, the kaon pair was not used. Another cut was used to prevent two reconstructed kaons from using the same daughter track. If two kaons shared a daughter track, one of them was cut using a procedure which compared the two K^0_S candidates and kept the candidate whose reconstructed parameters best matched those expected of a true K^0_S particle in two of three categories (smaller K^0_S DCA to primary vertex, smaller daughter-daughter DCA, and K^0_S mass closer to the PDG value [31]). This procedure was shown, using HIJING+GEANT3 simulations, to have a success rate of about 95% in selecting a true K^0_S particle over a fake one. More details about $K^0_S K^0_S$ analysis can be found in Refs. [16,32].

D. Proton selection

The single-particle cuts used in the proton analysis are summarized in Table I. The proton analysis used tracks with $0.7 < p_T < 4.0$ GeV/c . The lower p_T cut is used to suppress protons coming from weak decays and interactions with the detector material. Particle identification for p and $\bar{p}$ was performed using both TPC (for all momenta) and TOF (for $p > 0.8$ GeV/c). The proton purity was estimated using HIJING+GEANT3 simulations and was found to be greater than 95%. The used DCA criteria do not fully discriminate between primary protons and protons from weak decays. This may lead to a significant contamination from protons from

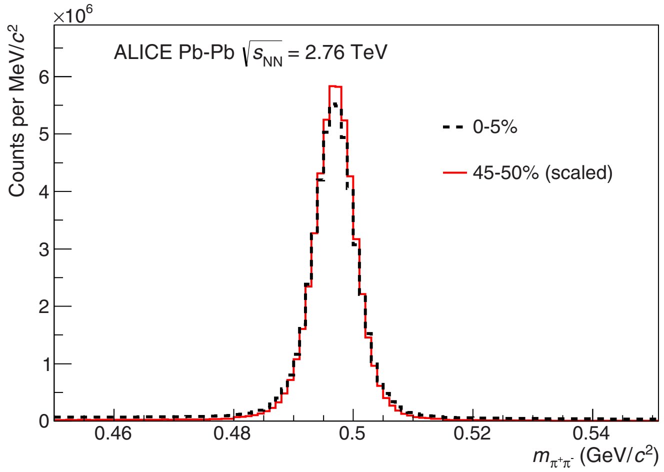

FIG. 2. (Color online) Invariant mass distribution of $\pi^+\pi^-$ pairs showing the K^0_S peak for two centrality intervals. The 45–50% centrality is scaled so that both distributions have the same integral in the range $0.480 < m_{\pi^+\pi^-} < 0.515$ GeV/c^2.

λ particles. The effect of this contamination is discussed in Sec. III D.

Regarding two-track selection criteria, pairs were required to have a separation of $|\Delta\eta| > 0.01$ or $|\Delta\varphi^*| > 0.045$ measured at the radial distance 1.2 m.

III. CONSTRUCTION OF THE CORRELATION FUNCTIONS AND FITTING PROCEDURES

The experimental two-particle correlation function is defined as $C(\mathbf{q}) = A(\mathbf{q})/B(\mathbf{q})$, where $A(\mathbf{q})$ is the measured distribution of same-event pair momentum difference, $\mathbf{q} = \mathbf{p}_1 - \mathbf{p}_2$, and $B(\mathbf{q})$ is the reference distribution of pairs from mixed events. The pairs in the denominator distribution $B(\mathbf{q})$ are constructed by taking a particle from one event and pairing it with a particle from another event with a similar centrality and primary vertex position along the beam direction. Each event is mixed with five (ten) others for the K^0_S ($\pi^\pm$, $\mathrm{K}^\pm$, p) analysis. The available statistics of proton pairs with low q ($<$0.2 GeV/c) allowed us to perform the analyses only for the one-dimensional correlation function $C(q)$, where $q = |\mathbf{q}|$ in the pair rest frame (PRF). In the case of pions and kaons, the statistics were high enough for three-dimensional studies, but these are beyond the scope of this paper; here, only the one-dimensional analysis is presented in order to compare results with heavier particles. The numerator and denominator are normalized such that $C(q) \to 1$ as $q \to \infty$. Pair cuts have been applied in exactly the same way for the same-event (signal) and mixed-event (background) pairs.

All correlation functions have been corrected for momentum resolution effects. The correction factors were determined using HIJING events to build simulated correlation functions using theoretical correlation functions as weights. The ratio of the correlation functions using HIJING generated momenta to those using HIJING+GEANT3 reconstructed momenta forms the correction factor.

For the analyses presented in this paper, the theoretical femtoscopic correlation function is defined as the square of the two-particle wave function averaged over the relative distance $\mathbf{r}^*$ of the emitters in the PRF. This is performed using the Koonin-Pratt equation [33,34]

$$C(q) = \int S(\mathbf{r}^*)|\Psi(q,\mathbf{r}^*)|^2 d^3\mathbf{r}^*. \tag{1}$$

For the one-dimensional analysis, we assume a spherically symmetric Gaussian distribution of the particle emitter spatial separation $\mathbf{r}^*$ in the PRF with size R_{inv} [35],

$$S(\mathbf{r}^*) \sim \exp\left(-\mathbf{r}^{*2}/4R_{\mathrm{inv}}^2\right). \tag{2}$$

The two-particle wave function is (anti)symmetrized for identical bosons (fermions) and may include terms incorporating Coulomb or strong final-state interactions, depending on the type of particles being studied.

The methods used in constructing and fitting the various correlation functions are discussed separately below.

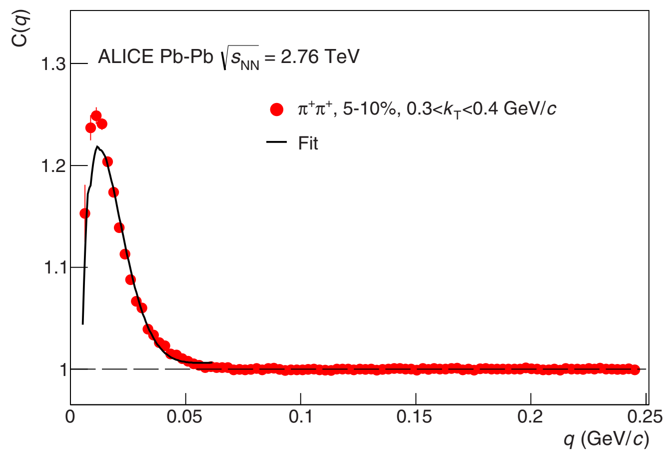

FIG. 3. (Color online) Example correlation function with fit for $\pi^+\pi^+$ for centrality 5–10% and $\langle k_\mathrm{T}\rangle = 0.35$ GeV/c. Statistical uncertainties are shown as thin lines.

A. Pions

Pion correlation functions were fitted using the Bowler-Sinyukov formula [36,37]:

$$C(q) = N\{1 - \lambda + \lambda K(q)[1 + \exp(-R_{\mathrm{inv}}^2 q^2)]\}, \tag{3}$$

where N is the normalization factor. The λ parameter (also used in the other analyses) can be affected by long-lived resonances, coherent sources [19,38,39], and non-Gaussian features of the particle-emission distribution. $K(q)$ is a symmetrized K factor calculated according to Refs. [19,37] as

$$K(q) = C(\mathrm{QS} + \mathrm{Coulomb})/C(\mathrm{QS}), \tag{4}$$

where $C(\mathrm{QS})$ and $C(\mathrm{QS} + \mathrm{Coulomb})$ are the theoretical correlation functions calculated with THERMINATOR 2 [40] using the quantum statistics ("QS") and "QS+Coulomb" weights (i.e., squared wave function), respectively [41]. The effect of the strong interaction is neglected here, since for like-sign pions, the contribution is small for the expected source sizes [41]. Figure 3 shows an example $\pi^+\pi^+$ correlation function with the corresponding line of best fit. More details about the pion analysis may be found in Ref. [42].

B. Charged kaons

Figure 4 shows an example $\mathrm{K}^\pm\mathrm{K}^\pm$ correlation function with the corresponding line of best fit. A purity correction was applied to the correlation function according to

$$C_{\mathrm{corrected}} = (C_{\mathrm{raw}} - 1 + P)/P, \tag{5}$$

where the pair purity P is taken from Fig. 1. $\mathrm{K}^\pm\mathrm{K}^\pm$ correlation functions were fitted using the Bowler-Sinyukov formula of Eq. (3); the procedure is essentially the same as for pions. There are no available experimental data for $\mathrm{K}^\pm\mathrm{K}^\pm$ strong FSI. The influence of the strong interaction to the correlation function was estimated with the s-wave scattering length calculated within the fully dynamical lattice QCD [43]. The systematic uncertainty assigned to this effect was determined to be 4%.

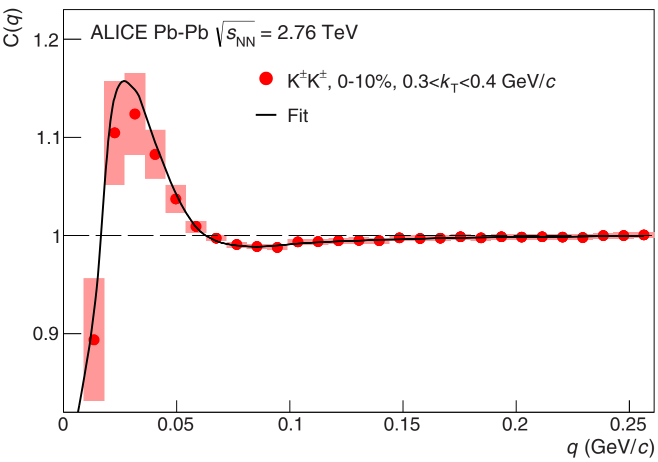

FIG. 4. (Color online) Example correlation function with fit for $K^{\pm}K^{\pm}$ for centrality 0–10% and $\langle k_T \rangle = 0.35$ GeV/c. Systematic uncertainties (boxes) are shown; statistical uncertainties are within the data markers. The main sources of systematic uncertainty are the momentum resolution correction and PID selection.

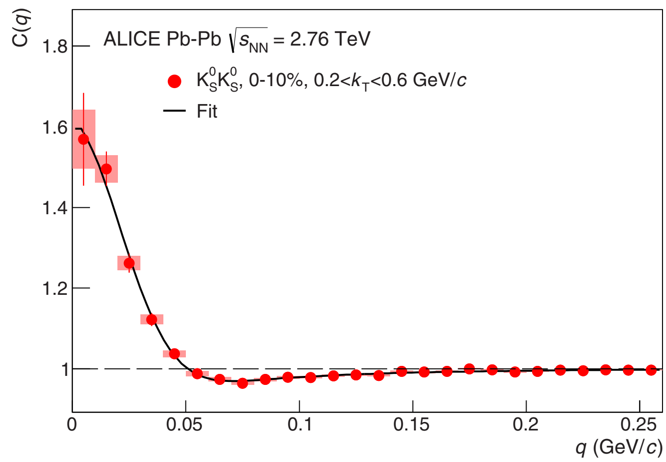

FIG. 5. (Color online) Example correlation function with fit for $K^0_S K^0_S$ for centrality 0–10% and $\langle k_T \rangle = 0.48$ GeV/c. Statistical (thin lines) and systematic (boxes) uncertainties are shown. The main source of systematic uncertainty is the variation of single-particle cuts.

C. Neutral kaons

Figure 5 shows an example $K^0_S K^0_S$ correlation function with the corresponding line of best fit. $K^0_S K^0_S$ correlation functions were fitted with a parametrization which includes Bose-Einstein statistics as well as strong final-state interactions (FSIs) [15,35],

$$C(q) = [1 - \lambda + \lambda C'(q)](a + bq), \tag{6}$$

where

$$C'(q) = 1 + e^{-q^2R^2} + C_{\text{strongFSI}}(q,R), \tag{7}$$

$$C_{\text{strongFSI}}(q,R) = \frac{1}{2}\left[\left|\frac{f(q)}{R}\right|^2 + \frac{4\text{Re} f(q)}{\sqrt{\pi}R} F_1(qR) - \frac{2\text{Im} f(q)}{R} F_2(qR)\right], \tag{8}$$

and

$$F_1(z) = \int_0^z dx \frac{e^{x^2-z^2}}{z}; \quad F_2(z) = \frac{1-e^{-z^2}}{z}. \tag{9}$$

$f(q)$ is the s-wave scattering amplitude for the $K^0\overline{K}^0$ system; we neglect the scattering for K^0K^0 and $\overline{K}^0\overline{K}^0$ due to small scattering lengths ≈0.1 fm [15]. The factor of 1/2 in Eq. (8) is due to the fact that half of the $K^0_S K^0_S$ pairs come from $K^0\overline{K}^0$. The strong FSI have a significant effect on the $K^0\overline{K}^0$ contribution to the $K^0_S K^0_S$ correlation function due to the near-threshold resonances, $f_0(980)$ and $a_0(980)$. For the scattering amplitude, only s-wave contributions were taken into account; the higher-order corrections were small and therefore neglected [44]. The scattering amplitude $f(q)$ is calculated using a two-channel parametrization which accounts for the elastic transition $K^0\overline{K}^0 \to K^0\overline{K}^0$ and the inelastic transition $K^+K^- \to K^0\overline{K}^0$ (see Ref. [15] for more detailed expressions describing the fit function). Equation (6) also includes an additional factor to account for nonfemtoscopic background correlations at large q, with a and b being free parameters in the fit.

D. Protons

Figure 6 shows an example $\overline{\text{p}}\overline{\text{p}}$ correlation function with the corresponding line of best fit. The femtoscopic correlations of pp and $\overline{\text{p}}\overline{\text{p}}$ pairs are due to a combination of Fermi-Dirac statistics, Coulomb, and strong FSIs. A distinct maximum is seen at $q \approx 40$ MeV/c [35]; this enhancement is due to the strong interaction, as both quantum statistics and Coulomb interaction present a negative correlation. Due to the fact that feeddown from weak decays cannot be neglected in high-energy heavy-ion collisions, the effects of residual correlations related to the pΛ system are taken into account. The proton daughter of a Λ decay has similar momentum to the

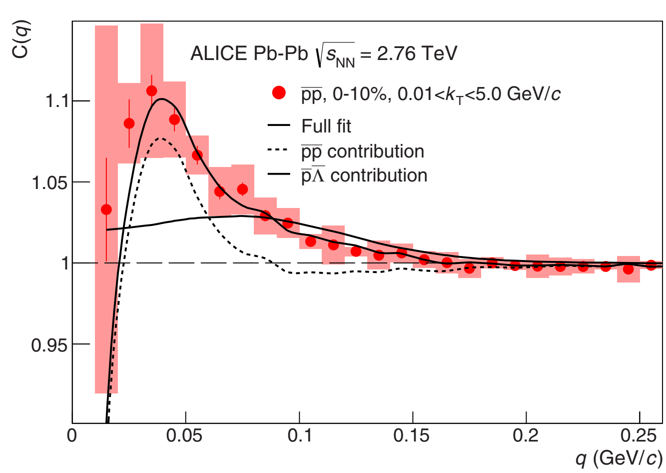

FIG. 6. (Color online) Example correlation function with fit for $\overline{\text{p}}\overline{\text{p}}$ for centrality 0–10% and $\langle k_T \rangle = 1.0$ GeV/c. Statistical (thin lines) and systematic (boxes) uncertainties are shown. The main source of systematic uncertainty is the variation of two-track cuts.

Λ itself and may survive the experimental selection for primary protons. Thus, it may contribute to the measured correlations by forming a pair with a primary proton. As can be seen in Fig. 6, attempting to fit the measured correlation functions with the theoretical pp ($\overline{\text{pp}}$) functions alone was unsuccessful due to the additional positive correlation observed in the range $60 < q < 160\ \text{MeV}/c$. Thus, a method of simultaneous fitting of pp ($\overline{\text{pp}}$) and pΛ ($\overline{\text{p}}\overline{\Lambda}$) correlations was applied. Contributions from heavier baryon-baryon pairs are not taken into account since the original correlation between the parent particles is not known due to unknown interaction parameters, for example for the $\Lambda\Lambda$ pair. Moreover such residual correlations are more smeared compared with pΛ because of larger decay momentum. In addition, the fraction of baryons heavier than Λ decaying to protons is smaller than the fraction of Λ's. Finally, comparing with baryon-antibaryon pairs analyzed in Ref. [45], the width of the correlation for baryon-baryon pairs is much smaller, and therefore the effect is much more smeared due to decay kinematics.

The experimental correlation function of pp and $\overline{\text{pp}}$ systems were fitted with [45]

$$C_{\text{meas}}(q_{\text{pp}}) = 1 + \lambda_{\text{pp}}[C_{\text{pp}}(q_{\text{pp}};R) - 1] + \lambda_{\text{p}\Lambda}[C_{\text{p}\Lambda}(q_{\text{pp}};R) - 1], \tag{10}$$

where λ_{pp} is the fraction of correlated pp pairs where both particles are primary, and $\lambda_{\text{p}\Lambda}$ is the fraction of correlated pp pairs where one particle is primary and the other is a daughter of Λ decay. The theoretical proton-proton correlation function was calculated as

$$C(q_{\text{pp}}) = \frac{1}{4}\left[\frac{\int S(\mathbf{r}^*)\frac{1}{2}\left|\Psi^{\text{S}}_{-\mathbf{q}_{\text{pp}}}(\mathbf{r}^*) + \Psi^{\text{S}}_{+\mathbf{q}_{\text{pp}}}(\mathbf{r}^*)\right|^2}{\int S(\mathbf{r}^*)}\right] + \frac{3}{4}\left[\frac{\int S(\mathbf{r}^*)\frac{1}{2}\left|\Psi^{\text{T}}_{-\mathbf{q}_{\text{pp}}}(\mathbf{r}^*) - \Psi^{\text{T}}_{+\mathbf{q}_{\text{pp}}}(\mathbf{r}^*)\right|^2}{\int S(\mathbf{r}^*)}\right]. \tag{11}$$

This formulation takes into account the necessary (anti)symmetrization of the wave function for a pp pair in the singlet (triplet) spin state with a corresponding weight of 1/4 (3/4). The pp pair wave function may be written as [44]

$$\Psi_{-\mathbf{q}_{\text{pp}}}(\mathbf{r}^*) = e^{i\delta_c}\sqrt{A_{\text{c}}(\eta)}\left[e^{-i\mathbf{q}_{\text{pp}}\cdot\mathbf{r}^*/2}F(-i\eta,1,i\xi) + f_{\text{c}}(q_{\text{pp}})\frac{\tilde{G}(\rho,\eta)}{|\mathbf{r}^*|}\right], \tag{12}$$

where $\mathbf{r}^*$ is the spatial separation of particle emitters at generally different emission moments in the PRF, $\delta_c = \arg\Gamma(1+i\eta)$ is the Coulomb s-wave phase shift, $A_{\text{c}}(\eta) = 2\pi\eta(e^{2\pi\eta}-1)^{-1}$ is the Gamow factor (also referred to as the Coulomb penetration factor), $\eta = (\frac{1}{2}aq_{\text{pp}})^{-1}$, $a = (\mu z_1 z_2 e^2)^{-1}$ is the two-particle Bohr radius taking into account the sign of the interaction ($a = 57.6$ fm for pp pair), F is the confluent hypergeometric function, $\xi = \frac{1}{2}q_{\text{pp}}r^*(1+\cos\theta^*)$, θ^* is the angle between $\mathbf{q}_{\text{pp}}$ and $\mathbf{r}^*$, $\tilde{G}$ is the combination of the regular and singular s-wave Coulomb functions, and $\rho = \frac{1}{2}q_{\text{pp}}r^*$. The amplitude of the low-energy s-wave elastic scattering due to the short range interaction $f_c(q_{\text{pp}})$ may be expressed as

$$f_c(q_{\text{pp}}) = \left[\frac{1}{f_0} + \frac{d_0 q_{\text{pp}}^2}{8} - \frac{1}{2}iq_{\text{pp}}A_{\text{c}}(\eta) - \frac{2}{a}h(\eta)\right]^{-1}, \tag{13}$$

where f_0 is the scattering length, d_0 is the effective radius of the interaction, $h(\eta) = [\psi(i\eta) + \psi(-i\eta) - \ln(\eta^2)]/2$, and ψ is the digamma function. For the pp system in the singlet (triplet) state, f_0 and d_0 are 7.77 fm (−5.4 fm) and 2.77 fm (1.7 fm).

For the feeddown term, the theoretical pΛ correlation function for a given $R_{\text{p}\Lambda}$ transformed into the pp momentum space is obtained from the Lednicky-Lyuboshitz model [35] and calculated as

$$C_{\text{p}\Lambda}(q_{\text{pp}};R_{\text{p}\Lambda}) = \sum_{q_{\text{p}\Lambda}} C_{\text{p}\Lambda}(q_{\text{p}\Lambda};R_{\text{p}\Lambda})T(q_{\text{pp}},q_{\text{p}\Lambda}) \Big/ \sum_{q_{\text{p}\Lambda}} T(q_{\text{pp}},q_{\text{p}\Lambda}), \tag{14}$$

where $C_{\text{p}\Lambda}(q_{\text{p}\Lambda};R_{\text{p}\Lambda}) = 1 + C_{\text{strongFSI}}(q_{\text{p}\Lambda};R_{\text{p}\Lambda})$, and $T(q_{\text{pp}},q_{\text{p}\Lambda})$ are the transformation factors related to Λ decay kinematics, calculated with THERMINATOR 2 [40]. Here, a spin-dependent version of Eq. (8) is used [35]:

$$C_{\text{strongFSI}}(q,R) = \sum_S \rho_S\left[\frac{1}{2}\left|\frac{f^S(q)}{R}\right|^2\left(1 - \frac{d_0^S}{2\sqrt{\pi}R}\right) + \frac{2\text{Re}f^S(q)}{\sqrt{\pi}R}F_1(qR) - \frac{\text{Im}f^S(q)}{R}F_2(qR)\right], \tag{15}$$

where $f^S(q)$ is the spin-dependent scattering amplitude, ρ_s is the fraction of pairs in each total spin state S, and d_0^S is the effective radius of the interaction. It is assumed that the radii of pp and pΛ sources are equal. Therefore, there are three free fit parameters in Eq. (10): λ_{pp}, $\lambda_{\text{p}\Lambda}$, and R. Theoretical pp and pΛ correlation functions were calculated using several values of the free parameters, and the fit function (for the set of parameters given during each fit iteration) was formed by a quadratic interpolation of the calculated correlation functions.

E. Systematic uncertainties

The effects of various sources of systematic uncertainty on the extracted fit parameters were studied as functions of centrality and k_{T}. Table II shows the minimum and maximum uncertainties from each source. The values of the total uncertainty are not necessarily equal to the sum of the individual uncertainties, as the latter can come from different centrality or k_{T} bins. All four analyses studied the effects of changing the selection criteria for the events, particles, and pairs used (variation of cut values up to ±25%) and varying the range of q values over which the fit is performed (variation of q limits up to ±25%). Uncertainties associated with momentum resolution corrections are included in the π, $\text{K}^{\pm}$, and p analyses; the K^0_{S} analysis also studied this and found the uncertainties to be negligible. The $\text{K}^{\pm}$, K^0_{S}, and p analyses encountered uncertainties associated with the nonflat background seen at large-q for high-k_{T} pairs in peripheral collisions [estimated by using different parametrizations (linear or polynomial) to fit the large-q region]. Strong FSI uncertainties

TABLE II. Minimal and maximal uncertainty values for various sources of systematic uncertainty (in percent). The λ for the proton analysis refers to the sum of λ_{pp} and $\lambda_{p\Lambda}$. Please note that each value is the minimum (maximum) uncertainty from a specific source, but each can be from a different centrality or k_T bin. Thus, the minimum (maximum) total uncertainties are greater (smaller) than (or equal to) the sum of the minimum (maximum) individual uncertainties. "n/a" denotes that the given descriptor of the systematic uncertainty is not applicable for the specific pair type, and "–" means that the contribution from the given source is negligible.

	$\pi^\pm$		$K^\pm$		K^0_S		p	
	R_{inv}	λ	R_{inv}	λ	R_{inv}	λ	R_{inv}	λ
Event/particle/pair selection	2–13	6	3–5	3–5	1–4	2–10	2–27	12–58
Non-flat background	–	–	0.2–5	0.2–5	0–5	0–4	2–3	1–9
Fit range	10	33	1–5	1–5	0–4	0–3	3–26	3–57
Strong FSI	–	–	4	4	1–2	5–10	n/a	n/a
Coulomb function	3	3	2	4	n/a	n/a	n/a	n/a
PID and purity	–	–	–	5–28	–	–	4–18	13–41
Momentum resolution	2	3	3–5	5–10	–	–	3	1–8
Fixing λ_{pp}	n/a	n/a	n/a	n/a	n/a	n/a	1–29	n/a
$R_{pp}/R_{p\Lambda}$ ratio	n/a	n/a	n/a	n/a	n/a	n/a	1–13	20–52
Total (quad. sum)	11–21	34	6–9	10–32	2–7	7–15	10–40	30–80

affect both kaon analyses. For K^0_S, the strong FSI uncertainty comes from the fact that several sets of $f_0(980)$ and $a_0(980)$ parameters are available [46–49]; each set is used to fit the data, the results are averaged, and the maximum difference was taken as the systematic error. The π and $K^\pm$ analyses have uncertainties associated with the choice of the Coulomb function used in the fitting procedure. The $K^\pm$ analysis had additional uncertainties due to the misidentification of particles and the associated purity correction. The p analysis also had uncertainties associated with the uncertainty in the $R_{pp}/R_{p\Lambda}$ ratio and attempts to fix the λ_{pp} parameter using the single-particle purity. All of the analyses were performed separately for the two different signs of the ALICE dipole magnetic field, but the resulting systematic uncertainty was found to be negligible in all cases.

Systematic uncertainties on correlation functions (Figs. 4–6) were derived from the variation of single- and two-particle cuts.

IV. RESULTS

Figures 7 and 8 present the extracted fit parameters from $\pi^\pm\pi^\pm$, $K^\pm K^\pm$, $K^0_S K^0_S$, and pp correlations for several intervals of centrality and transverse mass. Both statistical and systematic uncertainties are shown. The quality of the fits used to extract the shown parameters can be assessed using the χ^2/NDF values, which are in the ranges 1.2–5.0, 0.8–3.5, 0.6–1.5, and 0.8–3.2 for the pion, charged kaon, neutral kaon, and proton analyses, respectively.

Figure 7 shows the extracted λ parameters vs m_T for several centralities. The proton λ is the sum of λ_{pp} and $\lambda_{p\Lambda}$ from Eq. (10). The values for all species measured lie mostly in the range 0.3–0.7 and show no significant centrality dependence. The values of λ are less than unity due to long-lived resonances which dilute the correlation functions and also lead to non-Gaussian shapes of the correlation functions, especially in the one-dimensional case [20]. Results for kaons and protons are consistent with each other at similar m_T. Values of λ for pions are lower than for kaons due to the stronger influence of resonances; an additional cause could be a partial coherence of pions [19].

Figure 8 shows the extracted R_{inv} parameters vs m_T for several centralities. For overlapping m_T, the radius parameters are mostly consistent with each other within uncertainties, though the pion radii are generally larger than the kaon radii. The K^0_S radii are slightly higher than $K^\pm$ radii for central collisions, but the difference is less than the systematic uncertainties. The radius parameters show increasing size with increasing centrality as would be expected from a simple geometric picture of the collisions. They also show a decreasing size with increasing m_T as would be expected in the presence of collective radial flow [6]. Both of these dependencies can be seen in previous $\pi^\pm\pi^\pm$ femtoscopic measurements [4,5] and also reinforce the interpretation that collective flow is present in these collisions for pions, kaons (neutral and charged), and protons alike. Deviations from exact

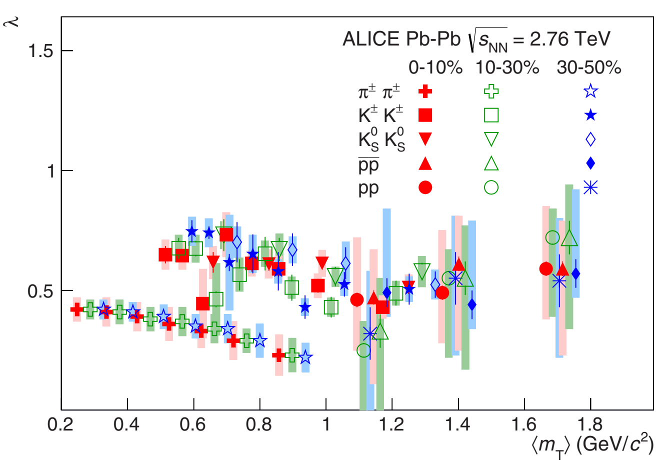

FIG. 7. (Color online) λ parameters [$\lambda_{pp} + \lambda_{p\Lambda}$ in the case of (anti)proton pairs] vs m_T for the three centralities considered for $\pi^\pm\pi^\pm$, $K^\pm K^\pm$, $K^0_S K^0_S$, pp, and $\overline{p}\overline{p}$. Statistical (thin lines) and systematic (boxes) uncertainties are shown. The m_T values for different centrality intervals are slightly offset for clarity.

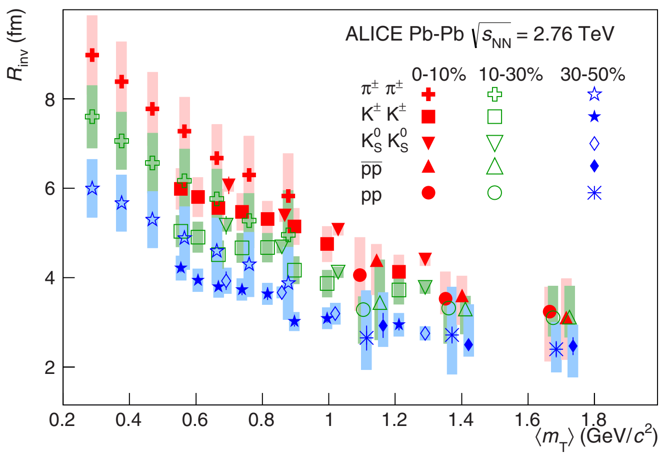

FIG. 8. (Color online) $R_{\rm inv}$ parameters vs $m_{\rm T}$ for the three centralities considered for $\pi^{\pm}\pi^{\pm}$, $K^{\pm}K^{\pm}$, $K^0_S K^0_S$, pp, and $\overline{p}\overline{p}$. Statistical (thin lines) and systematic (boxes) uncertainties are shown.

$m_{\rm T}$ scaling of $R_{\rm inv}$ can be explained as a consequence of the increase of the Lorentz factor with decreasing particle mass. In a hydrodynamic model [50], scaling is observed for the three-dimensional radii measured in the longitudinally comoving system (LCMS). The transformation from LCMS to PRF involves a boost along the outward direction only, where the boost value is proportional to the transverse velocity of the pair and inversely proportional to the particle mass (for similar $m_{\rm T}$). Thus, a smaller mass leads to an increase in the boosted $R_{\rm out}$ and, subsequently, $R_{\rm inv}$ in the PRF. Indeed, we observe such an effect in the data, as pion radii are systematically higher than kaon radii at the same $m_{\rm T}$.

A comparison of a hydrodynamic flow+kinetics model, HKM [14], with the measured $R_{\rm inv}$ and λ parameters for 0–5% centrality is shown in Fig. 9. The HKM values in Fig. 9 are specifically from $K^{\pm}K^{\pm}$, but the predictions for $K^0_S K^0_S$ and $K^{\pm}K^{\pm}$ are consistent with each other. For $R_{\rm inv}$, the charged kaon data show very good agreement with the predictions. The experimental data for the neutral kaons are again slightly higher than for the charged kaons, but this difference is still within systematic uncertainties. For λ, both sets of kaon data match the decreasing trend with increasing $k_{\rm T}$ exhibited by the HKM points, but the model slightly overpredicts the data. It is shown in Ref. [14] that the most important resonances for KK pairs, K*(890) and ϕ(1020), do not significantly influence the λ parameter (due to their low contribution), and the discrepancy between the model and experimental data can be explained by the lower experimental kaon purity and deviations of the experimental correlation function shape from a Gaussian distribution. For protons, the HKM prediction is compatible with the data. HKM calculations for one-dimensional pion radii are currently not available, but three-dimensional radii were reasonably reproduced by this model [51].

V. SUMMARY

Results from femtoscopic studies of $\pi^{\pm}\pi^{\pm}$, $K^{\pm}K^{\pm}$, $K^0_S K^0_S$, pp, and $\overline{p}\overline{p}$ correlations from Pb-Pb collisions at $\sqrt{s_{NN}} = 2.76$ TeV with ALICE at the LHC have been presented. The femtoscopic radii and λ parameters were extracted from one-dimensional correlation functions in terms of the invariant momentum difference. It was found that the emission source sizes of kaons and protons measured in these collisions exhibit transverse mass scaling within uncertainties, which is consistent with hydrodynamic model predictions assuming collective flow. The deviation from the scaling for the pions can be explained as a consequence of the increase of the Lorentz factor with decreasing particle mass during the transformation from LCMS to PRF systems [50]. The extracted λ parameters are found to be less than unity, as is expected due to long-lived resonances and non-Gaussian correlation functions. The predictions of the hydrokinetic model (HKM) for the one-dimensional femtoscopic radii for charged and neutral kaons and protons coincide well with the observations.

ACKNOWLEDGMENTS

The ALICE Collaboration would like to thank all its engineers and technicians for their invaluable contributions to the construction of the experiment and the CERN accelerator teams for the outstanding performance of the LHC complex. The ALICE Collaboration gratefully acknowledges the resources and support provided by all Grid centers and the Worldwide LHC Computing Grid (WLCG) collaboration. The ALICE Collaboration acknowledges the following funding agencies for their support in building and running the ALICE detector: State Committee of Science, World Federation of Scientists (WFS) and Swiss Fonds Kidagan,

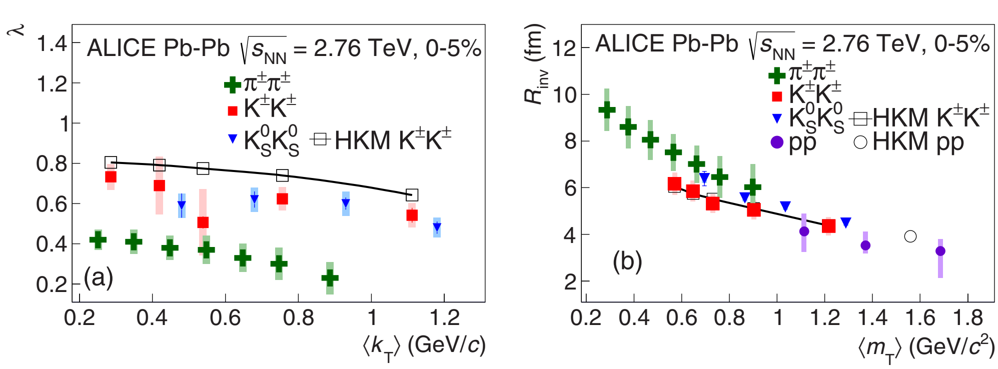

FIG. 9. (Color online) Comparison of the HKM model (see text) with measured kaon λ (a) and $R_{\rm inv}$ (b) parameters for 0–5% centrality. Statistical (thin lines) and systematic (boxes) uncertainties are shown.

Armenia, Conselho Nacional de Desenvolvimento Científico e Tecnológico (CNPq), Financiadora de Estudos e Projetos (FINEP), Fundação de Amparo à Pesquisa do Estado de São Paulo (FAPESP); National Natural Science Foundation of China (NSFC), the Chinese Ministry of Education (CMOE) and the Ministry of Science and Technology of China (MSTC); Ministry of Education and Youth of the Czech Republic; Danish Natural Science Research Council, the Carlsberg Foundation and the Danish National Research Foundation; The European Research Council under the European Community's Seventh Framework Programme; Helsinki Institute of Physics and the Academy of Finland; French CNRS-IN2P3, the "Region Pays de Loire," "Region Alsace," "Region Auvergne" and CEA, France; German Bundesministerium für Bildung, Wissenschaft, Forschung und Technologie (BMBF) and the Helmholtz Association; General Secretariat for Research and Technology, Ministry of Development, Greece; Hungarian Orszagos Tudomanyos Kutatasi Alappgrammok (OTKA) and National Office for Research and Technology (NKTH); Department of Atomic Energy and Department of Science and Technology of the Government of India; Istituto Nazionale di Fisica Nucleare (INFN) and Centro Fermi - Museo Storico della Fisica e Centro Studi e Ricerche "Enrico Fermi," Italy; MEXT Grant-in-Aid for Specially Promoted Research, Japan; Joint Institute for Nuclear Research, Dubna; National Research Foundation of Korea (NRF); Consejo Nacional de Cienca y Tecnologia (CONACYT), Direccion General de Asuntos del Personal Academico (DGAPA), México, Amerique Latine Formation academique - European Commission (ALFA-EC) and the EPLANET Program (European Particle Physics Latin American Network); Stichting voor Fundamenteel Onderzoek der Materie (FOM) and the Nederlandse Organisatie voor Wetenschappelijk Onderzoek (NWO), Netherlands; Research Council of Norway (NFR); National Science Centre, Poland; Ministry of National Education/Institute for Atomic Physics and National Council of Scientific Research in Higher Education (CNCSI-UEFISCDI), Romania; Ministry of Education and Science of Russian Federation, Russian Academy of Sciences, Russian Federal Agency of Atomic Energy, Russian Federal Agency for Science and Innovations and The Russian Foundation for Basic Research; Ministry of Education of Slovakia; Department of Science and Technology, South Africa; Centro de Investigaciones Energeticas, Medioambientales y Tecnologicas (CIEMAT), E-Infrastructure shared between Europe and Latin America (EELA), Ministerio de Economía y Competitividad (MINECO) of Spain, Xunta de Galicia (Consellería de Educación), Centro de Aplicaciones Tecnológicas y Desarrollo Nuclear (CEADEN), Cubaenergía, Cuba, and IAEA (International Atomic Energy Agency); Swedish Research Council (VR) and Knut & Alice Wallenberg Foundation (KAW); Ukraine Ministry of Education and Science; United Kingdom Science and Technology Facilities Council (STFC); The United States Department of Energy, the United States National Science Foundation, the State of Texas, and the State of Ohio; Ministry of Science, Education and Sports of Croatia and Unity through Knowledge Fund, Croatia; Council of Scientific and Industrial Research (CSIR), New Delhi, India.

[1] G. Goldhaber, S. Goldhaber, W.-Y. Lee, and A. Pais, Influence of Bose-Einstein statistics on the anti-proton proton annihilation process, Phys. Rev. **120**, 300 (1960).
[2] G. Kopylov and M. Podgoretsky, Correlations of identical particles emitted by highly excited nuclei, Sov. J. Nucl. Phys. **15**, 219 (1972).
[3] G. I. Kopylov, Like particle correlations as a tool to study the multiple production mechanism, Phys. Lett. B **50**, 472 (1974).
[4] M. A. Lisa, S. Pratt, R. Soltz, and U. Wiedemann, Femtoscopy in relativistic heavy ion collisions, Annu. Rev. Nucl. Part. Sci. **55**, 357 (2005).
[5] K. Aamodt *et al.* (ALICE Collaboration), Two-pion Bose-Einstein correlations in central Pb-Pb collisions at $\sqrt{s_{NN}} =$ 2.76 TeV, Phys. Lett. B **696**, 328 (2011).
[6] S. Akkelin and Y. Sinyukov, The HBT interferometry of expanding sources, Phys. Lett. B **356**, 525 (1995).
[7] A. Makhlin and Y. Sinyukov, Hydrodynamics of hadron matter under pion interferometric microscope, Z. Phys. C **39**, 69 (1988).
[8] I. Bearden *et al.* (NA44 Collaboration), Two Kaon Correlations in Central Pb+Pb Collisions at 158 AGeV/c, Phys. Rev. Lett. **87**, 112301 (2001).
[9] S. Afanasiev, T. Anticic, B. Baatar, D. Barna, J. Bartke *et al.* (NA49 Collaboration), Bose-Einstein correlations of charged kaons in central Pb+Pb collisions at E(beam) = 158 GeV per nucleon, Phys. Lett. B **557**, 157 (2003).
[10] D. Adamova *et al.* (CERES Collaboration), Beam energy and centrality dependence of two pion Bose-Einstein correlations at SPS energies, Nucl. Phys. A **714**, 124 (2003).
[11] J. Adams *et al.* (STAR Collaboration), Identified Particle Distributions in pp and Au + Au Collisions at $\sqrt{s_{NN}} = 200$ GeV, Phys. Rev. Lett. **92**, 112301 (2004).
[12] L. Adamczyk *et al.* (STAR Collaboration), Freeze-out dynamics via charged kaon femtoscopy in $\sqrt{s_{NN}} = 200$ GeV central Au + Au collisions, Phys. Rev. C **88**, 034906 (2013).
[13] S. Afanasiev *et al.* (PHENIX Collaboration), Kaon Interferometric Probes of Space-Time Evolution in Au + Au Collisions at $\sqrt{s_{NN}} = 200$ GeV, Phys. Rev. Lett. **103**, 142301 (2009).
[14] V. M. Shapoval, P. Braun-Munzinger, Iu. A. Karpenko, and Yu. M. Sinyukov, Femtoscopy correlations of kaons in Pb + Pb collisions at LHC within hydrokinetic model, Nucl. Phys. A **929**, 1 (2014).
[15] B. Abelev *et al.* (STAR Collaboration), Neutral kaon interferometry in Au + Au collisions at $\sqrt{s_{NN}} = 200$ GeV, Phys. Rev. C **74**, 054902 (2006).
[16] B. Abelev *et al.* (ALICE Collaboration), $K^0_s - K^0_s$ correlations in pp collisions at $\sqrt{s} = 7$ TeV from the LHC ALICE experiment, Phys. Lett. B **717**, 151 (2012).
[17] B. Abelev *et al.* (ALICE Collaboration), Charged kaon femtoscopic correlations in pp collisions at $\sqrt{s} = 7$ TeV, Phys. Rev. D **87**, 052016 (2013).

[18] A. Adare, S. Afanasiev, C. Aidala, N. Ajitanand, Y. Akiba *et al.*, Systematic study of charged-pion and kaon femtoscopy in Au + Au collisions at $\sqrt{s_{NN}} = 200$ GeV, Phys. Rev. C **92**, 034914 (2015).
[19] B. B. Abelev *et al.* (ALICE Collaboration), Two and three-pion quantum statistics correlations in Pb-Pb collisions at $\sqrt{s_{NN}} = 2.76$ TeV at the LHC, Phys. Rev. C **89**, 024911 (2014).
[20] B. B. Abelev *et al.* (ALICE Collaboration), Freeze-out radii extracted from three-pion cumulants in pp, p-Pb and Pb-Pb collisions at the LHC, Phys. Lett. B **739**, 139 (2014).
[21] CMS Collaboration, Femtoscopy with identified charged hadrons in pp, pPb, and peripheral PbPb collisions at LHC energies, Tech. Report CMS-PAS-HIN-14-013, CERN, Geneva, 2014. https://cds.cern.ch/record/1703272.
[22] H. Gos, Proton proton, anti-proton anti-proton, proton anti-proton correlations in Au + Au collisions measured by STAR at RHIC, Eur. Phys. J. C **49**, 75 (2007).
[23] K. Aamodt *et al.* (ALICE Collaboration), The ALICE experiment at the CERN LHC, J. Instrum. **3**, S08002 (2008).
[24] B. Abelev *et al.* (ALICE Collaboration), Centrality determination of Pb-Pb collisions at $\sqrt{s_{NN}} = 2.76$ TeV with ALICE, Phys. Rev. C **88**, 044909 (2013).
[25] G. Dellacasa *et al.* (ALICE Collaboration), ALICE: Technical design report of the time projection chamber, Geneva, 2000. http://cds.cern.ch/record/451098. CERN-OPEN-2000-183.
[26] B. Alessandro *et al.* (ALICE Collaboration), ALICE: Physics performance report, volume II, J. Phys. G **32**, 1295 (2006).
[27] P. Cortese *et al.* (ALICE Collaboration), ALICE: Addendum to the technical design report of the time of flight system (TOF), Geneva, 2000. http://cds.cern.ch/record/545834. CERN-LHCC-2002-016.
[28] B. B. Abelev *et al.* (ALICE Collaboration), Performance of the ALICE Experiment at the CERN LHC, Int. J. Mod. Phys. A **29**, 1430044 (2014).
[29] X.-N. Wang and M. Gyulassy, HIJING: A Monte Carlo model for multiple jet production in pp, pA and AA collisions, Phys. Rev. D **44**, 3501 (1991).
[30] R. Brun, F. Carminati, and S. Giani, GEANT Detector Description and Simulation Tool, 1994. CERN-W5013, CERN-W-5013.
[31] K. Olive *et al.* (Particle Data Group Collaboration), Review of Particle Physics, Chin. Phys. C **38**, 090001 (2014).
[32] M. Steinpreis, Neutral kaon femtoscopy in Pb-Pb collisions at $\sqrt{s_{NN}} = 2.76$ TeV at the LHC with ALICE, PhD. thesis, The Ohio State University, 2014. https://rave.ohiolink.edu/etdc/view?acc_num=osu1417696971.
[33] S. Koonin, Proton Pictures of High-Energy Nuclear Collisions, Phys. Lett. B **70**, 43 (1977).
[34] S. Pratt, T. Csorgo, and J. Zimanyi, Detailed predictions for two pion correlations in ultrarelativistic heavy ion collisions, Phys. Rev. C **42**, 2646 (1990).
[35] R. Lednicky and V. Lyuboshits, Final State Interaction Effect on Pairing Correlations Between Particles with Small Relative Momenta, Sov. J. Nucl. Phys. **35**, 770 (1982).
[36] M. Bowler, Coulomb corrections to Bose-Einstein correlations have been greatly exaggerated, Phys. Lett. B **270**, 69 (1991).
[37] Y. Sinyukov, R. Lednicky, S. Akkelin, J. Pluta, and B. Erazmus, Coulomb corrections for interferometry analysis of expanding hadron systems, Phys. Lett. B **432**, 248 (1998).
[38] S. V. Akkelin, R. Lednicky, and Y. M. Sinyukov, Correlation search for coherent pion emission in heavy ion collisions, Phys. Rev. C **65**, 064904 (2002).
[39] U. A. Wiedemann and U. W. Heinz, Resonance contributions to HBT correlation radii, Phys. Rev. C **56**, 3265 (1997).
[40] M. Chojnacki, A. Kisiel, W. Florkowski, and W. Broniowski, THERMINATOR 2: THERMal heavy IoN generATOR 2, Comput. Phys. Commun. **183**, 746 (2012).
[41] R. Lednicky, Correlation femtoscopy, Nucl. Phys. A **774**, 189 (2006).
[42] J. Adam *et al.* (ALICE Collaboration), Centrality dependence of pion freeze-out radii in Pb-Pb collisions at $\sqrt{s_{NN}} = 2.76$ TeV, arXiv:1507.06842.
[43] S. R. Beane *et al.* (NPLQCD Collaboration), The K^+K^+ scattering length from lattice QCD, Phys. Rev. D **77**, 094507 (2008).
[44] R. Lednicky, Finite-size effects on two-particle production in continuous and discrete spectrum, Phys. Part. Nucl. **40**, 307 (2009).
[45] A. Kisiel, H. Zbroszczyk, and M. Szymanski, Extracting baryon-antibaryon strong interaction potentials from $p\bar{\Lambda}$ femtoscopic correlation function, Phys. Rev. C **89**, 054916 (2014).
[46] A. Martin, E. Ozmutlu, and E. Squires, The $\pi\pi$ and $K\bar{K}$ amplitudes, the S^* and the quark structure of 0^{++} resonances, Nucl. Phys. B **121**, 514 (1977).
[47] A. Antonelli (KLOE Collaboration), Radiative phi decays, eConf C020620, THAT06 (2002), arXiv:hep-ex/0209069.
[48] N. Achasov and V. Gubin, Analysis of the nature of the $\vec{\varphi}\gamma\pi\eta$ and $\vec{\varphi}\gamma\pi^0\pi^0$ decays, Phys. Rev. D **63**, 094007 (2001).
[49] N. Achasov and A. Kiselev, New analysis of the KLOE data on the $\vec{\varphi}\eta\pi^0\gamma$ decay, Phys. Rev. D **68**, 014006 (2003).
[50] A. Kisiel, M. Galazyn, and P. Bozek, Pion, kaon, and proton femtoscopy in Pb-Pb collisions at $\sqrt{s_{NN}} = 2.76$ TeV modeled in 3+1D hydrodynamics, Phys. Rev. C **90**, 064914 (2014).
[51] I. Karpenko, Y. Sinyukov, and K. Werner, Uniform description of bulk observables in the hydrokinetic model of $A + A$ collisions at the BNL Relativistic Heavy Ion Collider and the CERN Large Hadron Collider, Phys. Rev. C **87**, 024914 (2013).

J. Adam,[40] D. Adamová,[83] M. M. Aggarwal,[87] G. Aglieri Rinella,[36] M. Agnello,[111] N. Agrawal,[48] Z. Ahammed,[132] S. U. Ahn,[68] I. Aimo,[94,111] S. Aiola,[137] M. Ajaz,[16] A. Akindinov,[58] S. N. Alam,[132] D. Aleksandrov,[100] B. Alessandro,[111] D. Alexandre,[102] R. Alfaro Molina,[64] A. Alici,[105,12] A. Alkin,[3] J. Alme,[38] T. Alt,[43] S. Altinpinar,[18] I. Altsybeev,[131] C. Alves Garcia Prado,[120] C. Andrei,[78] A. Andronic,[97] V. Anguelov,[93] J. Anielski,[54] T. Antičić,[98] F. Antinori,[108] P. Antonioli,[105] L. Aphecetche,[113] H. Appelshäuser,[53] S. Arcelli,[28] N. Armesto,[17] R. Arnaldi,[111] I. C. Arsene,[22] M. Arslandok,[53] B. Audurier,[113] A. Augustinus,[36] R. Averbeck,[97] M. D. Azmi,[19] M. Bach,[43] A. Badalà,[107] Y. W. Baek,[44] S. Bagnasco,[111] R. Bailhache,[53]

R. Bala,[90] A. Baldisseri,[15] F. Baltasar Dos Santos Pedrosa,[36] R. C. Baral,[61] A. M. Barbano,[111] R. Barbera,[29] F. Barile,[33] G. G. Barnaföldi,[136] L. S. Barnby,[102] V. Barret,[70] P. Bartalini,[7] K. Barth,[36] J. Bartke,[117] E. Bartsch,[53] M. Basile,[28] N. Bastid,[70] S. Basu,[132] B. Bathen,[54] G. Batigne,[113] A. Batista Camejo,[70] B. Batyunya,[66] P. C. Batzing,[22] I. G. Bearden,[80] H. Beck,[53] C. Bedda,[111] N. K. Behera,[49,48] I. Belikov,[55] F. Bellini,[28] H. Bello Martinez,[2] R. Bellwied,[122] R. Belmont,[135] E. Belmont-Moreno,[64] V. Belyaev,[76] G. Bencedi,[136] S. Beole,[27] I. Berceanu,[78] A. Bercuci,[78] Y. Berdnikov,[85] D. Berenyi,[136] R. A. Bertens,[57] D. Berzano,[36,27] L. Betev,[36] A. Bhasin,[90] I. R. Bhat,[90] A. K. Bhati,[87] B. Bhattacharjee,[45] J. Bhom,[128] L. Bianchi,[122] N. Bianchi,[72] C. Bianchin,[135,57] J. Bielčík,[40] J. Bielčíková,[83] A. Bilandzic,[80] R. Biswas,[4] S. Biswas,[79] S. Bjelogrlic,[57] F. Blanco,[10] D. Blau,[100] C. Blume,[53] F. Bock,[74,93] A. Bogdanov,[76] H. Bøggild,[80] L. Boldizsár,[136] M. Bombara,[41] J. Book,[53] H. Borel,[15] A. Borissov,[96] M. Borri,[82] F. Bossú,[65] M. Botje,[81] E. Botta,[27] S. Böttger,[52] P. Braun-Munzinger,[97] M. Bregant,[120] T. Breitner,[52] T. A. Broker,[53] T. A. Browning,[95] M. Broz,[40] E. J. Brucken,[46] E. Bruna,[111] G. E. Bruno,[33] D. Budnikov,[99] H. Buesching,[53] S. Bufalino,[111,36] P. Buncic,[36] O. Busch,[93,128] Z. Buthelezi,[65] J. B. Butt,[16] J. T. Buxton,[20] D. Caffarri,[36] X. Cai,[7] H. Caines,[137] L. Calero Diaz,[72] A. Caliva,[57] E. Calvo Villar,[103] P. Camerini,[26] F. Carena,[36] W. Carena,[36] J. Castillo Castellanos,[15] A. J. Castro,[125] E. A. R. Casula,[25] C. Cavicchioli,[36] C. Ceballos Sanchez,[9] J. Cepila,[40] P. Cerello,[111] J. Cerkala,[115] B. Chang,[123] S. Chapeland,[36] M. Chartier,[124] J. L. Charvet,[15] S. Chattopadhyay,[132] S. Chattopadhyay,[101] V. Chelnokov,[3] M. Cherney,[86] C. Cheshkov,[130] B. Cheynis,[130] V. Chibante Barroso,[36] D. D. Chinellato,[121] P. Chochula,[36] K. Choi,[96] M. Chojnacki,[80] S. Choudhury,[132] P. Christakoglou,[81] C. H. Christensen,[80] P. Christiansen,[34] T. Chujo,[128] S. U. Chung,[96] Z. Chunhui,[57] C. Cicalo,[106] L. Cifarelli,[12,28] F. Cindolo,[105] J. Cleymans,[89] F. Colamaria,[33] D. Colella,[33,59] A. Collu,[25] M. Colocci,[28] G. Conesa Balbastre,[71] Z. Conesa del Valle,[51] M. E. Connors,[137] J. G. Contreras,[11,40] T. M. Cormier,[84] Y. Corrales Morales,[27] I. Cortés Maldonado,[2] P. Cortese,[32] M. R. Cosentino,[120] F. Costa,[36] P. Crochet,[70] R. Cruz Albino,[11] E. Cuautle,[63] L. Cunqueiro,[36] T. Dahms,[92,37] A. Dainese,[108] A. Danu,[62] D. Das,[101] I. Das,[51,101] S. Das,[4] A. Dash,[121] S. Dash,[48] S. De,[120] A. De Caro,[31,12] G. de Cataldo,[104] J. de Cuveland,[43] A. De Falco,[25] D. De Gruttola,[12,31] N. De Marco,[111] S. De Pasquale,[31] A. Deisting,[97,93] A. Deloff,[77] E. Dénes,[136] G. D'Erasmo,[33] D. Di Bari,[33] A. Di Mauro,[36] P. Di Nezza,[72] M. A. Diaz Corchero,[10] T. Dietel,[89] P. Dillenseger,[53] R. Divià,[36] Ø. Djuvsland,[18] A. Dobrin,[57,81] T. Dobrowolski,[77,*] D. Domenicis Gimenez,[120] B. Dönigus,[53] O. Dordic,[22] A. K. Dubey,[132] A. Dubla,[57] L. Ducroux,[130] P. Dupieux,[70] R. J. Ehlers,[137] D. Elia,[104] H. Engel,[52] B. Erazmus,[36,113] I. Erdemir,[53] F. Erhardt,[129] D. Eschweiler,[43] B. Espagnon,[51] M. Estienne,[113] S. Esumi,[128] J. Eum,[96] D. Evans,[102] S. Evdokimov,[112] G. Eyyubova,[40] L. Fabbietti,[37,92] D. Fabris,[108] J. Faivre,[71] A. Fantoni,[72] M. Fasel,[74] L. Feldkamp,[54] D. Felea,[62] A. Feliciello,[111] G. Feofilov,[131] J. Ferencei,[83] A. Fernández Téllez,[2] E. G. Ferreiro,[17] A. Ferretti,[27] A. Festanti,[30] V. J. G. Feuillard,[70,15] J. Figiel,[117] M. A. S. Figueredo,[124] S. Filchagin,[99] D. Finogeev,[56] F. M. Fionda,[104] E. M. Fiore,[33] M. G. Fleck,[93] M. Floris,[36] S. Foertsch,[65] P. Foka,[97] S. Fokin,[100] E. Fragiacomo,[110] A. Francescon,[30,36] U. Frankenfeld,[97] U. Fuchs,[36] C. Furget,[71] A. Furs,[56] M. Fusco Girard,[31] J. J. Gaardhøje,[80] M. Gagliardi,[27] A. M. Gago,[103] M. Gallio,[27] D. R. Gangadharan,[74] P. Ganoti,[88] C. Gao,[7] C. Garabatos,[97] E. Garcia-Solis,[13] C. Gargiulo,[36] P. Gasik,[92,37] M. Germain,[113] A. Gheata,[36] M. Gheata,[62,36] P. Ghosh,[132] S. K. Ghosh,[4] P. Gianotti,[72] P. Giubellino,[111,36] P. Giubilato,[30] E. Gladysz-Dziadus,[117] P. Glässel,[93] A. Gomez Ramirez,[52] P. González-Zamora,[10] S. Gorbunov,[43] L. Görlich,[117] S. Gotovac,[116] V. Grabski,[64] L. K. Graczykowski,[134] K. L. Graham,[102] A. Grelli,[57] A. Grigoras,[36] C. Grigoras,[36] V. Grigoriev,[76] A. Grigoryan,[1] S. Grigoryan,[66] B. Grinyov,[3] N. Grion,[110] J. F. Grosse-Oetringhaus,[36] J.-Y. Grossiord,[130] R. Grosso,[36] F. Guber,[56] R. Guernane,[71] B. Guerzoni,[28] K. Gulbrandsen,[80] H. Gulkanyan,[1] T. Gunji,[127] A. Gupta,[90] R. Gupta,[90] R. Haake,[54] Ø. Haaland,[18] C. Hadjidakis,[51] M. Haiduc,[62] H. Hamagaki,[127] G. Hamar,[136] A. Hansen,[80] J. W. Harris,[137] H. Hartmann,[43] A. Harton,[13] D. Hatzifotiadou,[105] S. Hayashi,[127] S. T. Heckel,[53] M. Heide,[54] H. Helstrup,[38] A. Herghelegiu,[78] G. Herrera Corral,[11] B. A. Hess,[35] K. F. Hetland,[38] T. E. Hilden,[46] H. Hillemanns,[36] B. Hippolyte,[55] R. Hosokawa,[128] P. Hristov,[36] M. Huang,[18] T. J. Humanic,[20] N. Hussain,[45] T. Hussain,[19] D. Hutter,[43] D. S. Hwang,[21] R. Ilkaev,[99] I. Ilkiv,[77] M. Inaba,[128] C. Ionita,[36] M. Ippolitov,[76,100] M. Irfan,[19] M. Ivanov,[97] V. Ivanov,[85] V. Izucheev,[112] P. M. Jacobs,[74] S. Jadlovska,[115] C. Jahnke,[120] H. J. Jang,[68] M. A. Janik,[134] P. H. S. Y. Jayarathna,[122] C. Jena,[30] S. Jena,[122] R. T. Jimenez Bustamante,[97] P. G. Jones,[102] H. Jung,[44] A. Jusko,[102] P. Kalinak,[59] A. Kalweit,[36] J. Kamin,[53] J. H. Kang,[138] V. Kaplin,[76] S. Kar,[132] A. Karasu Uysal,[69] O. Karavichev,[56] T. Karavicheva,[56] E. Karpechev,[56] U. Kebschull,[52] R. Keidel,[139] D. L. D. Keijdener,[57] M. Keil,[36] K. H. Khan,[16] M. M. Khan,[19] P. Khan,[101] S. A. Khan,[132] A. Khanzadeev,[85] Y. Kharlov,[112] B. Kileng,[38] B. Kim,[138] D. W. Kim,[44,68] D. J. Kim,[123] H. Kim,[138] J. S. Kim,[44] M. Kim,[44] M. Kim,[138] S. Kim,[21] T. Kim,[138] S. Kirsch,[43] I. Kisel,[43] S. Kiselev,[58] A. Kisiel,[134] G. Kiss,[136] J. L. Klay,[6] C. Klein,[53] J. Klein,[93] C. Klein-Bösing,[54] A. Kluge,[36] M. L. Knichel,[93] A. G. Knospe,[118] T. Kobayashi,[128] C. Kobdaj,[114] M. Kofarago,[36] T. Kollegger,[97,43] A. Kolojvari,[131] V. Kondratiev,[131] N. Kondratyeva,[76] E. Kondratyuk,[112] A. Konevskikh,[56] M. Kopcik,[115] C. Kouzinopoulos,[36] O. Kovalenko,[77] V. Kovalenko,[131] M. Kowalski,[117] S. Kox,[71] G. Koyithatta Meethaleveedu,[48] J. Kral,[123] I. Králik,[59] A. Kravčáková,[41] M. Krelina,[40] M. Kretz,[43] M. Krivda,[102,59] F. Krizek,[83] E. Kryshen,[36] M. Krzewicki,[43] A. M. Kubera,[20] V. Kučera,[83] T. Kugathasan,[36] C. Kuhn,[55] P. G. Kuijer,[81] I. Kulakov,[43] J. Kumar,[48] L. Kumar,[79,87] P. Kurashvili,[77] A. Kurepin,[56] A. B. Kurepin,[56] A. Kuryakin,[99] S. Kushpil,[83] M. J. Kweon,[50] Y. Kwon,[138] S. L. La Pointe,[111] P. La Rocca,[29] C. Lagana Fernandes,[120] I. Lakomov,[36] R. Langoy,[42] C. Lara,[52] A. Lardeux,[15] A. Lattuca,[27] E. Laudi,[36] R. Lea,[26] L. Leardini,[93] G. R. Lee,[102] S. Lee,[138] I. Legrand,[36] R. C. Lemmon,[82] V. Lenti,[104] E. Leogrande,[57] I. León Monzón,[119] M. Leoncino,[27] P. Lévai,[136] S. Li,[7,70] X. Li,[14] J. Lien,[42] R. Lietava,[102] S. Lindal,[22] V. Lindenstruth,[43] C. Lippmann,[97] M. A. Lisa,[20] H. M. Ljunggren,[34] D. F. Lodato,[57] P. I. Loenne,[18] V. R. Loggins,[135] V. Loginov,[76] C. Loizides,[74] X. Lopez,[70] E. López Torres,[9] A. Lowe,[136] P. Luettig,[53] M. Lunardon,[30] G. Luparello,[26] P. H. F. N. D. Luz,[120] A. Maevskaya,[56] M. Mager,[36]

S. Mahajan,[90] S. M. Mahmood,[22] A. Maire,[55] R. D. Majka,[137] M. Malaev,[85] I. Maldonado Cervantes,[63] L. Malinina,[66] D. Mal'Kevich,[58] P. Malzacher,[97] A. Mamonov,[99] L. Manceau,[111] V. Manko,[100] F. Manso,[70] V. Manzari,[104,36] M. Marchisone,[27] J. Mareš,[60] G. V. Margagliotti,[26] A. Margotti,[105] J. Margutti,[57] A. Marín,[97] C. Markert,[118] M. Marquard,[53] N. A. Martin,[97] J. Martin Blanco,[113] P. Martinengo,[36] M. I. Martínez,[2] G. Martínez García,[113] M. Martinez Pedreira,[36] Y. Martynov,[3] A. Mas,[120] S. Masciocchi,[97] M. Masera,[27] A. Masoni,[106] L. Massacrier,[113] A. Mastroserio,[33] H. Masui,[128] A. Matyja,[117] C. Mayer,[117] J. Mazer,[125] M. A. Mazzoni,[109] D. Mcdonald,[122] F. Meddi,[24] A. Menchaca-Rocha,[64] E. Meninno,[31] J. Mercado Pérez,[93] M. Meres,[39] Y. Miake,[128] M. M. Mieskolainen,[46] K. Mikhaylov,[58,66] L. Milano,[36] J. Milosevic,[133,22] L. M. Minervini,[104,23] A. Mischke,[57] A. N. Mishra,[49] D. Miśkowiec,[97] J. Mitra,[132] C. M. Mitu,[62] N. Mohammadi,[57] B. Mohanty,[79,132] L. Molnar,[55] L. Montaño Zetina,[11] E. Montes,[10] M. Morando,[30] D. A. Moreira De Godoy,[113,54] S. Moretto,[30] A. Morreale,[113] A. Morsch,[36] V. Muccifora,[72] E. Mudnic,[116] D. Mühlheim,[54] S. Muhuri,[132] M. Mukherjee,[132] J. D. Mulligan,[137] M. G. Munhoz,[120] S. Murray,[65] L. Musa,[36] J. Musinsky,[59] B. K. Nandi,[48] R. Nania,[105] E. Nappi,[104] M. U. Naru,[16] C. Nattrass,[125] K. Nayak,[79] T. K. Nayak,[132] S. Nazarenko,[99] A. Nedosekin,[58] L. Nellen,[63] F. Ng,[122] M. Nicassio,[97] M. Niculescu,[62,36] J. Niedziela,[36] B. S. Nielsen,[80] S. Nikolaev,[100] S. Nikulin,[100] V. Nikulin,[85] F. Noferini,[12,105] P. Nomokonov,[66] G. Nooren,[57] J. C. C. Noris,[2] J. Norman,[124] A. Nyanin,[100] J. Nystrand,[18] H. Oeschler,[93] S. Oh,[137] S. K. Oh,[67] A. Ohlson,[36] A. Okatan,[69] T. Okubo,[47] L. Olah,[136] J. Oleniacz,[134] A. C. Oliveira Da Silva,[120] M. H. Oliver,[137] J. Onderwaater,[97] C. Oppedisano,[111] A. Ortiz Velasquez,[63] A. Oskarsson,[34] J. Otwinowski,[117] K. Oyama,[93] M. Ozdemir,[53] Y. Pachmayer,[93] P. Pagano,[31] G. Paić,[63] C. Pajares,[17] S. K. Pal,[132] J. Pan,[135] A. K. Pandey,[48] D. Pant,[48] P. Papcun,[115] V. Papikyan,[1] G. S. Pappalardo,[107] P. Pareek,[49] W. J. Park,[97] S. Parmar,[87] A. Passfeld,[54] V. Paticchio,[104] R. N. Patra,[132] B. Paul,[101] T. Peitzmann,[57] H. Pereira Da Costa,[15] E. Pereira De Oliveira Filho,[120] D. Peresunko,[100,76] C. E. Pérez Lara,[81] E. Perez Lezama,[43] V. Peskov,[53] Y. Pestov,[5] V. Petráček,[40] V. Petrov,[112] M. Petrovici,[78] C. Petta,[29] S. Piano,[110] M. Pikna,[39] P. Pillot,[113] O. Pinazza,[105,36] L. Pinsky,[122] D. B. Piyarathna,[122] M. Płoskoń,[74] M. Planinic,[129] J. Pluta,[134] S. Pochybova,[136] P. L. M. Podesta-Lerma,[119] M. G. Poghosyan,[86] B. Polichtchouk,[112] N. Poljak,[129] W. Poonsawat,[114] A. Pop,[78] S. Porteboeuf-Houssais,[70] J. Porter,[74] J. Pospisil,[83] S. K. Prasad,[4] R. Preghenella,[105,36] F. Prino,[111] C. A. Pruneau,[135] I. Pshenichnov,[56] M. Puccio,[111] G. Puddu,[25] P. Pujahari,[135] V. Punin,[99] J. Putschke,[135] H. Qvigstad,[22] A. Rachevski,[110] S. Raha,[4] S. Rajput,[90] J. Rak,[123] A. Rakotozafindrabe,[15] L. Ramello,[32] R. Raniwala,[91] S. Raniwala,[91] S. S. Räsänen,[46] B. T. Rascanu,[53] D. Rathee,[87] K. F. Read,[125] J. S. Real,[71] K. Redlich,[77] R. J. Reed,[135] A. Rehman,[18] P. Reichelt,[53] F. Reidt,[93,36] X. Ren,[7] R. Renfordt,[53] A. R. Reolon,[72] A. Reshetin,[56] F. Rettig,[43] J.-P. Revol,[12] K. Reygers,[93] V. Riabov,[85] R. A. Ricci,[73] T. Richert,[34] M. Richter,[22] P. Riedler,[36] W. Riegler,[36] F. Riggi,[29] C. Ristea,[62] A. Rivetti,[111] E. Rocco,[57] M. Rodríguez Cahuantzi,[2] A. Rodriguez Manso,[81] K. Røed,[22] E. Rogochaya,[66] D. Rohr,[43] D. Röhrich,[18] R. Romita,[124] F. Ronchetti,[72] L. Ronflette,[113] P. Rosnet,[70] A. Rossi,[30,36] F. Roukoutakis,[88] A. Roy,[49] C. Roy,[55] P. Roy,[101] A. J. Rubio Montero,[10] R. Rui,[26] R. Russo,[27] E. Ryabinkin,[100] Y. Ryabov,[85] A. Rybicki,[117] S. Sadovsky,[112] K. Šafařík,[36] B. Sahlmuller,[53] P. Sahoo,[49] R. Sahoo,[49] S. Sahoo,[61] P. K. Sahu,[61] J. Saini,[132] S. Sakai,[72] M. A. Saleh,[135] C. A. Salgado,[17] J. Salzwedel,[20] S. Sambyal,[90] V. Samsonov,[85] X. Sanchez Castro,[55] L. Šándor,[59] A. Sandoval,[64] M. Sano,[128] G. Santagati,[29] D. Sarkar,[132] E. Scapparone,[105] F. Scarlassara,[30] R. P. Scharenberg,[95] C. Schiaua,[78] R. Schicker,[93] C. Schmidt,[97] H. R. Schmidt,[35] S. Schuchmann,[53] J. Schukraft,[36] M. Schulc,[40] T. Schuster,[137] Y. Schutz,[113,36] K. Schwarz,[97] K. Schweda,[97] G. Scioli,[28] E. Scomparin,[111] R. Scott,[125] K. S. Seeder,[120] J. E. Seger,[86] Y. Sekiguchi,[127] D. Sekihata,[47] I. Selyuzhenkov,[97] K. Senosi,[65] J. Seo,[96,67] E. Serradilla,[64,10] A. Sevcenco,[62] A. Shabanov,[56] A. Shabetai,[113] O. Shadura,[3] R. Shahoyan,[36] A. Shangaraev,[112] A. Sharma,[90] N. Sharma,[61,125] K. Shigaki,[47] K. Shtejer,[9,27] Y. Sibiriak,[100] S. Siddhanta,[106] K. M. Sielewicz,[36] T. Siemiarczuk,[77] D. Silvermyr,[84,34] C. Silvestre,[71] G. Simatovic,[129] G. Simonetti,[36] R. Singaraju,[132] R. Singh,[79] S. Singha,[79,132] V. Singhal,[132] B. C. Sinha,[132] T. Sinha,[101] B. Sitar,[39] M. Sitta,[32] T. B. Skaali,[22] M. Slupecki,[123] N. Smirnov,[137] R. J. M. Snellings,[57] T. W. Snellman,[123] C. Søgaard,[34] R. Soltz,[75] J. Song,[96] M. Song,[138] Z. Song,[7] F. Soramel,[30] S. Sorensen,[125] M. Spacek,[40] E. Spiriti,[72] I. Sputowska,[117] M. Spyropoulou-Stassinaki,[88] B. K. Srivastava,[95] J. Stachel,[93] I. Stan,[62] G. Stefanek,[77] M. Steinpreis,[20] E. Stenlund,[34] G. Steyn,[65] J. H. Stiller,[93] D. Stocco,[113] P. Strmen,[39] A. A. P. Suaide,[120] T. Sugitate,[47] C. Suire,[51] M. Suleymanov,[16] R. Sultanov,[58] M. Šumbera,[83] T. J. M. Symons,[74] A. Szabo,[39] A. Szanto de Toledo,[120,*] I. Szarka,[39] A. Szczepankiewicz,[36] M. Szymanski,[134] J. Takahashi,[121] N. Tanaka,[128] M. A. Tangaro,[33] J. D. Tapia Takaki,[51,†] A. Tarantola Peloni,[53] M. Tarhini,[51] M. Tariq,[19] M. G. Tarzila,[78] A. Tauro,[36] G. Tejeda Muñoz,[2] A. Telesca,[36] K. Terasaki,[127] C. Terrevoli,[30,25] B. Teyssier,[130] J. Thäder,[74,97] D. Thomas,[118] R. Tieulent,[130] A. R. Timmins,[122] A. Toia,[53] S. Trogolo,[111] V. Trubnikov,[3] W. H. Trzaska,[123] T. Tsuji,[127] A. Tumkin,[99] R. Turrisi,[108] T. S. Tveter,[22] K. Ullaland,[18] A. Uras,[130] G. L. Usai,[25] A. Utrobicic,[129] M. Vajzer,[83] M. Vala,[59] L. Valencia Palomo,[70] S. Vallero,[27] J. Van Der Maarel,[57] J. W. Van Hoorne,[36] M. van Leeuwen,[57] T. Vanat,[83] P. Vande Vyvre,[36] D. Varga,[136] A. Vargas,[2] M. Vargyas,[123] R. Varma,[48] M. Vasileiou,[88] A. Vasiliev,[100] A. Vauthier,[71] V. Vechernin,[131] A. M. Veen,[57] M. Veldhoen,[57] A. Velure,[18] M. Venaruzzo,[73] E. Vercellin,[27] S. Vergara Limón,[2] R. Vernet,[8] M. Verweij,[135] L. Vickovic,[116] G. Viesti,[30,*] J. Viinikainen,[123] Z. Vilakazi,[126] O. Villalobos Baillie,[102] A. Vinogradov,[100] L. Vinogradov,[131] Y. Vinogradov,[99,*] T. Virgili,[31] V. Vislavicius,[34] Y. P. Viyogi,[132] A. Vodopyanov,[66] M. A. Völkl,[93] K. Voloshin,[58] S. A. Voloshin,[135] G. Volpe,[136,36] B. von Haller,[36] I. Vorobyev,[92,37] D. Vranic,[97,36] J. Vrláková,[41] B. Vulpescu,[70] A. Vyushin,[99] B. Wagner,[18] J. Wagner,[97] H. Wang,[57] M. Wang,[7,113] Y. Wang,[93] D. Watanabe,[128] Y. Watanabe,[127] M. Weber,[36] S. G. Weber,[97] J. P. Wessels,[54] U. Westerhoff,[54] J. Wiechula,[35] J. Wikne,[22] M. Wilde,[54] G. Wilk,[77] J. Wilkinson,[93] M. C. S. Williams,[105] B. Windelband,[93] M. Winn,[93] C. G. Yaldo,[135] H. Yang,[57] P. Yang,[7] S. Yano,[47] Z. Yin,[7] H. Yokoyama,[128] I.-K. Yoo,[96] V. Yurchenko,[3] I. Yushmanov,[100] A. Zaborowska,[134] V. Zaccolo,[80] A. Zaman,[16] C. Zampolli,[105] H. J. C. Zanoli,[120] S. Zaporozhets,[66] N. Zardoshti,[102] A. Zarochentsev,[131] P. Závada,[60]

N. Zaviyalov,[99] H. Zbroszczyk,[134] I. S. Zgura,[62] M. Zhalov,[85] H. Zhang,[18,7] X. Zhang,[74] Y. Zhang,[7] C. Zhao,[22] N. Zhigareva,[58] D. Zhou,[7] Y. Zhou,[80,57] Z. Zhou,[18] H. Zhu,[18,7] J. Zhu,[113,7] X. Zhu,[7] A. Zichichi,[12,28] A. Zimmermann,[93] M. B. Zimmermann,[54,36] G. Zinovjev,[3] and M. Zyzak[43]

(ALICE Collaboration)

[1]*A.I. Alikhanyan National Science Laboratory (Yerevan Physics Institute) Foundation, Yerevan, Armenia*
[2]*Benemérita Universidad Autónoma de Puebla, Puebla, Mexico*
[3]*Bogolyubov Institute for Theoretical Physics, Kiev, Ukraine*
[4]*Bose Institute, Department of Physics and Centre for Astroparticle Physics and Space Science (CAPSS), Kolkata, India*
[5]*Budker Institute for Nuclear Physics, Novosibirsk, Russia*
[6]*California Polytechnic State University, San Luis Obispo, California, USA*
[7]*Central China Normal University, Wuhan, China*
[8]*Centre de Calcul de l'IN2P3, Villeurbanne, France*
[9]*Centro de Aplicaciones Tecnológicas y Desarrollo Nuclear (CEADEN), Havana, Cuba*
[10]*Centro de Investigaciones Energéticas Medioambientales y Tecnológicas (CIEMAT), Madrid, Spain*
[11]*Centro de Investigación y de Estudios Avanzados (CINVESTAV), Mexico City and Mérida, Mexico*
[12]*Centro Fermi - Museo Storico della Fisica e Centro Studi e Ricerche "Enrico Fermi," Rome, Italy*
[13]*Chicago State University, Chicago, Illinois, USA*
[14]*China Institute of Atomic Energy, Beijing, China*
[15]*Commissariat à l'Energie Atomique, IRFU, Saclay, France*
[16]*COMSATS Institute of Information Technology (CIIT), Islamabad, Pakistan*
[17]*Departamento de Física de Partículas and IGFAE, Universidad de Santiago de Compostela, Santiago de Compostela, Spain*
[18]*Department of Physics and Technology, University of Bergen, Bergen, Norway*
[19]*Department of Physics, Aligarh Muslim University, Aligarh, India*
[20]*Department of Physics, Ohio State University, Columbus, Ohio, USA*
[21]*Department of Physics, Sejong University, Seoul, South Korea*
[22]*Department of Physics, University of Oslo, Oslo, Norway*
[23]*Dipartimento di Elettrotecnica ed Elettronica del Politecnico, Bari, Italy*
[24]*Dipartimento di Fisica dell'Università 'La Sapienza' and Sezione INFN Rome, Italy*
[25]*Dipartimento di Fisica dell'Università and Sezione INFN, Cagliari, Italy*
[26]*Dipartimento di Fisica dell'Università and Sezione INFN, Trieste, Italy*
[27]*Dipartimento di Fisica dell'Università and Sezione INFN, Turin, Italy*
[28]*Dipartimento di Fisica e Astronomia dell'Università and Sezione INFN, Bologna, Italy*
[29]*Dipartimento di Fisica e Astronomia dell'Università and Sezione INFN, Catania, Italy*
[30]*Dipartimento di Fisica e Astronomia dell'Università and Sezione INFN, Padova, Italy*
[31]*Dipartimento di Fisica 'E.R. Caianiello' dell'Università and Gruppo Collegato INFN, Salerno, Italy*
[32]*Dipartimento di Scienze e Innovazione Tecnologica dell'Università del Piemonte Orientale and Gruppo Collegato INFN, Alessandria, Italy*
[33]*Dipartimento Interateneo di Fisica "M. Merlin" and Sezione INFN, Bari, Italy*
[34]*Division of Experimental High Energy Physics, University of Lund, Lund, Sweden*
[35]*Eberhard Karls Universität Tübingen, Tübingen, Germany*
[36]*European Organization for Nuclear Research (CERN), Geneva, Switzerland*
[37]*Excellence Cluster Universe, Technische Universität München, Munich, Germany*
[38]*Faculty of Engineering, Bergen University College, Bergen, Norway*
[39]*Faculty of Mathematics, Physics and Informatics, Comenius University, Bratislava, Slovakia*
[40]*Faculty of Nuclear Sciences and Physical Engineering, Czech Technical University in Prague, Prague, Czech Republic*
[41]*Faculty of Science, P.J. Šafárik University, Košice, Slovakia*
[42]*Faculty of Technology, Buskerud and Vestfold University College, Vestfold, Norway*
[43]*Frankfurt Institute for Advanced Studies, Johann Wolfgang Goethe-Universität Frankfurt, Frankfurt, Germany*
[44]*Gangneung-Wonju National University, Gangneung, South Korea*
[45]*Gauhati University, Department of Physics, Guwahati, India*
[46]*Helsinki Institute of Physics (HIP), Helsinki, Finland*
[47]*Hiroshima University, Hiroshima, Japan*
[48]*Indian Institute of Technology Bombay (IIT), Mumbai, India*
[49]*Indian Institute of Technology Indore, Indore (IITI), India*
[50]*Inha University, Incheon, South Korea*
[51]*Institut de Physique Nucléaire d'Orsay (IPNO), Université Paris-Sud, CNRS-IN2P3, Orsay, France*
[52]*Institut für Informatik, Johann Wolfgang Goethe-Universität Frankfurt, Frankfurt, Germany*

[53]*Institut für Kernphysik, Johann Wolfgang Goethe-Universität Frankfurt, Frankfurt, Germany*
[54]*Institut für Kernphysik, Westfälische Wilhelms-Universität Münster, Münster, Germany*
[55]*Institut Pluridisciplinaire Hubert Curien (IPHC), Université de Strasbourg, CNRS-IN2P3, Strasbourg, France*
[56]*Institute for Nuclear Research, Academy of Sciences, Moscow, Russia*
[57]*Institute for Subatomic Physics of Utrecht University, Utrecht, The Netherlands*
[58]*Institute for Theoretical and Experimental Physics, Moscow, Russia*
[59]*Institute of Experimental Physics, Slovak Academy of Sciences, Košice, Slovakia*
[60]*Institute of Physics, Academy of Sciences of the Czech Republic, Prague, Czech Republic*
[61]*Institute of Physics, Bhubaneswar, India*
[62]*Institute of Space Science (ISS), Bucharest, Romania*
[63]*Instituto de Ciencias Nucleares, Universidad Nacional Autónoma de México, Mexico City, Mexico*
[64]*Instituto de Física, Universidad Nacional Autónoma de México, Mexico City, Mexico*
[65]*iThemba LABS, National Research Foundation, Somerset West, South Africa*
[66]*Joint Institute for Nuclear Research (JINR), Dubna, Russia*
[67]*Konkuk University, Seoul, South Korea*
[68]*Korea Institute of Science and Technology Information, Daejeon, South Korea*
[69]*KTO Karatay University, Konya, Turkey*
[70]*Laboratoire de Physique Corpusculaire (LPC), Clermont Université, Université Blaise Pascal, CNRS–IN2P3, Clermont-Ferrand, France*
[71]*Laboratoire de Physique Subatomique et de Cosmologie, Université Grenoble-Alpes, CNRS-IN2P3, Grenoble, France*
[72]*Laboratori Nazionali di Frascati, INFN, Frascati, Italy*
[73]*Laboratori Nazionali di Legnaro, INFN, Legnaro, Italy*
[74]*Lawrence Berkeley National Laboratory, Berkeley, California, USA*
[75]*Lawrence Livermore National Laboratory, Livermore, California, USA*
[76]*Moscow Engineering Physics Institute, Moscow, Russia*
[77]*National Centre for Nuclear Studies, Warsaw, Poland*
[78]*National Institute for Physics and Nuclear Engineering, Bucharest, Romania*
[79]*National Institute of Science Education and Research, Bhubaneswar, India*
[80]*Niels Bohr Institute, University of Copenhagen, Copenhagen, Denmark*
[81]*Nikhef, Nationaal Instituut voor Subatomaire Fysica, Amsterdam, The Netherlands*
[82]*Nuclear Physics Group, STFC Daresbury Laboratory, Daresbury, United Kingdom*
[83]*Nuclear Physics Institute, Academy of Sciences of the Czech Republic, Řež u Prahy, Czech Republic*
[84]*Oak Ridge National Laboratory, Oak Ridge, Tennessee, USA*
[85]*Petersburg Nuclear Physics Institute, Gatchina, Russia*
[86]*Physics Department, Creighton University, Omaha, Nebraska, USA*
[87]*Physics Department, Panjab University, Chandigarh, India*
[88]*Physics Department, University of Athens, Athens, Greece*
[89]*Physics Department, University of Cape Town, Cape Town, South Africa*
[90]*Physics Department, University of Jammu, Jammu, India*
[91]*Physics Department, University of Rajasthan, Jaipur, India*
[92]*Physik Department, Technische Universität München, Munich, Germany*
[93]*Physikalisches Institut, Ruprecht-Karls-Universität Heidelberg, Heidelberg, Germany*
[94]*Politecnico di Torino, Turin, Italy*
[95]*Purdue University, West Lafayette, Indiana, USA*
[96]*Pusan National University, Pusan, South Korea*
[97]*Research Division and ExtreMe Matter Institute EMMI, GSI Helmholtzzentrum für Schwerionenforschung, Darmstadt, Germany*
[98]*Rudjer Bošković Institute, Zagreb, Croatia*
[99]*Russian Federal Nuclear Center (VNIIEF), Sarov, Russia*
[100]*Russian Research Centre Kurchatov Institute, Moscow, Russia*
[101]*Saha Institute of Nuclear Physics, Kolkata, India*
[102]*School of Physics and Astronomy, University of Birmingham, Birmingham, United Kingdom*
[103]*Sección Física, Departamento de Ciencias, Pontificia Universidad Católica del Perú, Lima, Peru*
[104]*Sezione INFN, Bari, Italy*
[105]*Sezione INFN, Bologna, Italy*
[106]*Sezione INFN, Cagliari, Italy*
[107]*Sezione INFN, Catania, Italy*
[108]*Sezione INFN, Padova, Italy*
[109]*Sezione INFN, Rome, Italy*
[110]*Sezione INFN, Trieste, Italy*
[111]*Sezione INFN, Turin, Italy*

[112]*SSC IHEP of NRC Kurchatov Institute, Protvino, Russia*
[113]*SUBATECH, Ecole des Mines de Nantes, Université de Nantes, CNRS-IN2P3, Nantes, France*
[114]*Suranaree University of Technology, Nakhon Ratchasima, Thailand*
[115]*Technical University of Košice, Košice, Slovakia*
[116]*Technical University of Split FESB, Split, Croatia*
[117]*The Henryk Niewodniczanski Institute of Nuclear Physics, Polish Academy of Sciences, Cracow, Poland*
[118]*The University of Texas at Austin, Physics Department, Austin, Texas, USA*
[119]*Universidad Autónoma de Sinaloa, Culiacán, Mexico*
[120]*Universidade de São Paulo (USP), São Paulo, Brazil*
[121]*Universidade Estadual de Campinas (UNICAMP), Campinas, Brazil*
[122]*University of Houston, Houston, Texas, USA*
[123]*University of Jyväskylä, Jyväskylä, Finland*
[124]*University of Liverpool, Liverpool, United Kingdom*
[125]*University of Tennessee, Knoxville, Tennessee, USA*
[126]*University of the Witwatersrand, Johannesburg, South Africa*
[127]*University of Tokyo, Tokyo, Japan*
[128]*University of Tsukuba, Tsukuba, Japan*
[129]*University of Zagreb, Zagreb, Croatia*
[130]*Université de Lyon, Université Lyon 1, CNRS/IN2P3, IPN-Lyon, Villeurbanne, France*
[131]*V. Fock Institute for Physics, St. Petersburg State University, St. Petersburg, Russia*
[132]*Variable Energy Cyclotron Centre, Kolkata, India*
[133]*Vinča Institute of Nuclear Sciences, Belgrade, Serbia*
[134]*Warsaw University of Technology, Warsaw, Poland*
[135]*Wayne State University, Detroit, Michigan, USA*
[136]*Wigner Research Centre for Physics, Hungarian Academy of Sciences, Budapest, Hungary*
[137]*Yale University, New Haven, Connecticut, USA*
[138]*Yonsei University, Seoul, South Korea*
[139]*Zentrum für Technologietransfer und Telekommunikation (ZTT), Fachhochschule Worms, Worms, Germany*

[*]Deceased.
[†]Also at University of Kansas, Lawrence, KS, United States.